



ELSEVIER

Available online at [www.sciencedirect.com](http://www.sciencedirect.com)

SCIENCE @ DIRECT®

Computerized Medical Imaging and Graphics 27 (2003) 351–362

Computerized  
Medical Imaging  
and Graphics

[www.elsevier.com/locate/compmedimag](http://www.elsevier.com/locate/compmedimag)

## 3DVIEWNIX-AVS: a software package for the separate visualization of arteries and veins in CE-MRA images

Tianhu Lei, Jayaram K. Udupa\*, Dewey Odhner, László G. Nyúl, Punam K. Saha

*Medical Image Processing Group, Department of Radiology, University of Pennsylvania, 4th floor, Blockley Hall,  
423 Guardian Drive, Philadelphia, PA 19104-6021, USA*

Received 27 September 2002; accepted 10 December 2002

### Abstract

Our earlier study developed a computerized method, based on fuzzy connected object delineation principles and algorithms, for artery and vein separation in contrast enhanced Magnetic Resonance Angiography (CE-MRA) images. This paper reports its current development—a software package—for routine clinical use. The software package, termed 3DVIEWNIX-AVS, consists of the following major operational parts: (1) converting data from DICOM3 to 3DVIEWNIX format, (2) previewing slices and creating VOI and MIP Shell, (3) segmenting vessel, (4) separating artery and vein, (5) shell rendering vascular structures and creating animations.

This package has been applied to EPIX Medical Inc's CE-MRA data (AngioMark MS-325). One hundred and thirty-five original CE-MRA data sets (of 52 patients) from 6 hospitals have been processed. In all case studies, unified parameter settings produce correct artery–vein separation. The current package is running on a Pentium PC under Linux and the total computation time per study is about 3 min.

The strengths of this software package are (1) minimal user interaction, (2) minimal anatomic knowledge requirements on human vascular system, (3) clinically required speed, (4) free entry to any operational stages, (5) reproducible, reliable, high quality of results, and (6) cost effective computer implementation. To date, it seems to be the only software package (using an image processing approach) available for artery and vein separation of the human vascular system for routine use in a clinical setting.

© 2003 Elsevier Science Ltd. All rights reserved.

*Keywords:* Image segmentation; Artery–vein separation; Fuzzy connectedness; Contrast enhanced magnetic resonance angiography; Visualization systems

### 1. Introduction

#### 1.1. Contrast enhanced MRA

Magnetic Resonance Angiography (MRA) has established itself as an important technique complementary to conventional angiography [1–3]. It facilitates high quality depiction of the cerebral vasculature and has become an accepted clinical procedure. However, its effectiveness for abdominal and peripheral imaging is limited due to some intrinsic limitations of the technique itself. The complicated flow patterns and in-plane flow may result in signal voids which can lead to an overestimate of stenosis [4].

Extracellular contrast agents (e.g. Gd-DTPA) [5–7] have considerably increased the clinical applicability of conventional MRA. Because shortened T1 of blood provides contrast (rather than the flow dynamics), contrast

enhanced MRA (CE-MRA) is less sensitive to flow conditions. Also, high contrast can be obtained in shorter examination times, enabling breath hold sequences which reduce motion artifacts. The shortcoming of such contrast agents is their rapid diffusion into extracellular space, which limits the imaging window to a few minutes since the background signal increases as well.

Intravascular contrast agents (e.g. AngioMark MS-325 or NS 100150) [8,9] also exhibit strong T1 shortening properties in blood. In comparison to extracellular agents, intravascular agents offer a much longer blood residence time, higher concentration within the blood pool, and a reduction of extravasation into myocardium. This primary advantage allows acquisition of steady-state images of the arteries and veins over multiple body regions with excellent spatial resolution. The drawback of this contrast agent, however, is the venous contamination of arterial images, which can significantly hamper diagnosis of the main arterial branches [10,11].

\* Corresponding author. Tel.: +1-215-662-6780; fax: +1-215-898-9145.  
E-mail address: [jay@mipg.upenn.edu](mailto:jay@mipg.upenn.edu) (J.K. Udupa).

Thus, the development of artery–vein separation techniques directly from the steady-state CE-MRA images can potentially overcome this problem, and has, therefore, considerable significance clinically.

### 1.2. Approaches to artery–vein separation

The strategies adopted in the past for artery–vein separation include both acquisition methods and post-processing techniques [12]. Among the current developments, the former include phase-contrast and time-resolved acquisition approaches [13–15], and the latter cover correlation analysis and graph searching methods [16–18]. The shortcomings of these approaches, in general, are the limitations of their applications and costs. Among data acquisition approaches, phase-contrast methods [13] are limited to the case where the blood flow directions in artery and vein are opposite to each other. In time-resolved acquisition approaches [14,15], the image must be acquired during the first pass of a contrast agent or accomplished by cardiac gating. The development of image processing approaches to artery–vein separation has recently begun [16–22]. Among these, correlation analysis [16] requires seven or eight MRA data sets in a single breathhold for a 3D angiogram of the lung. In graph searching approaches [17], the node costs require 3D edge strength and a model of preferred branch direction. The enhanced artery visualization method [18] is limited to the segmentation of a small number of the main overlapping veins in the peripheral vasculature. Therefore, a more general approach for artery–vein separation is desirable.

### 1.3. Software package implementation of artery–vein separation

Our earlier study [19–22] developed a near automatic procedure for separating arteries and veins in CE-MRA image data and an optimal method for 3D visualization of vascular structures. The separation process utilizes fuzzy connected object delineation principles and algorithms. The first step of this separation process is the segmentation of the entire vessel structure from the background and other clutter via absolute fuzzy connectedness. The second step is to separate artery from vein within this entire vessel structure via iterative relative fuzzy connectedness. Then shell rendering is applied to the vessel structures obtained in the above two steps for visualization.

The above segmentation, separation, as well as rendition procedures are implemented by a newly developed software package, termed 3DVIEWNIX-AVS and based on the general software system 3DVIEWNIX<sup>1</sup> [23], for routine clinical use. This software package consists of the following

major operational parts: (1) converting data from DICOM3 to 3DVIEWNIX format, (2) previewing slices and creating VOI and MIP Shell<sup>2</sup> (3) segmenting vessel, (4) separating artery and vein, (5) shell rendering vascular structures and creating animations. It has been applied to EPIX Medical Inc's CE-MRA data (AngioMark MS-325). One hundred and thirty-five original CE-MRA data sets (of 52 patients) from 6 hospitals have been processed. In all case studies, unified parameter settings produce correct artery–vein separation. The current package runs on a Pentium PC under Linux and the total operation time per study is about 3 min.

This paper is organized as follows. Section 2 briefly reviews the theory of artery–vein separation developed in our earlier study. Section 3 describes the implementation methods in detail. The software package, 3DVIEWNIX-AVS, is presented in Section 4. The results obtained by using this package are shown in Section 5. Conclusions are given in Section 6. A preliminary version of this paper [21] was presented at the SPIE Medical Imaging conference.

## 2. Theory

For the convenience and completeness of description, this section briefly reviews the theory of artery–vein separation—the fuzzy connected object delineation principles and algorithms—developed in our earlier study. It is the basis of the implementation methods (Section 3) and the software package (Section 4). In this section, after describing several fuzzy concepts, absolute fuzzy connectedness is introduced for vessel segmentation and iterative relative fuzzy connectedness is described for artery–vein separation. More details of the theory can be found in our earlier reports [19–22,24–27].

### 2.1. Fuzzy adjacency and fuzzy affinity

We refer to a three-dimensional digital image as a scene and represent it by a pair  $\mathcal{C} = (C, f)$ , where  $C = \{c \mid -b_j \leq c_j \leq b_j \text{ for some } b = (b_1, b_2, b_3) \in \mathbb{Z}_+^3\}$  is a rectangular three-dimensional array of voxels  $c = (c_1, c_2, c_3)$  ( $\mathbb{Z}_+^3$  is a set of three-tuples of positive integers), and  $f$  is a function, called scene intensity, with  $C$  as its domain and with a set of integers as its range.

*Fuzzy adjacency* ( $\alpha, \mu_\alpha$ ). Independent of any image data, we think of the digital space defined by the voxels as having a fuzzy adjacency relation. We denote the fuzzy adjacency relation by  $\alpha$  and the degree of adjacency assigned to a pair  $(c, d)$  of voxels by  $\mu_\alpha(c, d)$ . The fuzzy adjacency relation assigns to every pair  $(c, d)$  of voxels a value between zero and one. The closer  $c$  and  $d$  are to each

<sup>1</sup> An open, transportable, multidimensional, multimodality, multiparametric imaging software system that is not specific to any particular application.

<sup>2</sup> VOI: volume of interest, MIP: maximum intensity projection, Shell: a data structure used by 3DVIEWNIX to represent fuzzy objects.

other, the greater is this number. In our studies, we use

$$\mu_\alpha(c, d) = \begin{cases} 1, & \|c - d\| \leq 1, \\ 0, & \text{otherwise.} \end{cases} \quad (1)$$

where  $\|c - d\|$  denotes the distance between  $c$  and  $d$ .

*Fuzzy affinity* ( $\kappa, \mu_\kappa$ ). For a given scene  $\mathcal{C} = (C, f)$ , we define another local fuzzy relation called *affinity*, denoted  $\kappa$ , on voxels. The strength  $\mu_\kappa(c, d)$  of this relation between any voxels  $c$  and  $d$  lies between zero and one and indicates how the image elements ‘hang together’ locally in the scene.  $\mu_\kappa(c, d)$  is a function of  $\mu_\alpha(c, d)$  and of  $f(x)$  and  $f(y)$  for all voxels  $x$  and  $y$  in a certain neighborhood of  $c$  and  $d$ , respectively. In our studies, we use

$$\mu_\kappa(c, d) = \mu_\alpha(c, d) \sqrt{\mu_{\phi_s}(c, d) \mu_{\psi_s}(c, d)}, \quad (2)$$

where  $\mu_{\phi_s}$  and  $\mu_{\psi_s}$  are object-feature-based and homogeneity-based components of affinity, respectively.

The design of  $\mu_{\phi_s}$  and  $\mu_{\psi_s}$  adopts the following strategies: (1) If both  $c$  and  $d$  have high object belongingness and both have low background belongingness, then they have a high object-feature-based affinity (the only feature used here is the intensity of voxels). (2) If the intensities of the corresponding voxels within the neighborhoods of  $c$  and  $d$  are close (i.e. both  $c$  and  $d$  are inside a homogeneous object region), then they have a high homogeneity-based affinity. More details about the functional forms of  $\mu_{\phi_s}$  and  $\mu_{\psi_s}$  are given in our earlier papers [19–22,24–27]. Since the size of this neighborhood changes over the scene domain,  $\mu_\kappa(c, d)$  is shift-variant over the scene.

*Scale*. Scale in  $\mathcal{C}$  at any voxel  $c \in C$  is defined as the radius  $r(c)$  of the largest ball centered at  $c$  which lies entirely inside the same homogeneous region. For computing affinity, the neighborhood defined by the scale value at different locations in the scene is utilized. Ref. [25] describes an algorithm which estimates  $r(c)$  for any  $\mathcal{C}$  based on the continuity of intensity homogeneity. This information (scale) leads to better fuzzy connectedness and object delineation (which are described below) than if just the voxels  $c$  and  $d$  (and their properties) are used in defining  $\mu_\kappa(c, d)$ .

## 2.2. Absolute fuzzy connectedness

*Fuzzy connectedness* ( $K, \mu_K$ ). ‘Hanging togetherness’ in a global sense is a global fuzzy relation on voxels called *fuzzy connectedness*, denoted  $K$ . The strength  $\mu_K(c, d)$  of this relation between any voxels  $c \in C$  and  $d \in C$  is determined as follows. There are numerous possible ‘paths’ within the scene domain  $C$  between  $c$  and  $d$ . A path  $p_{cd}$  between  $c$  and  $d$  is a sequence  $(c^1, c^2, \dots, c^m)$  of  $m \geq 2$  voxels, all in  $C$ , such that  $c^1 = c$ ,  $c^m = d$ . The ‘strength of connectedness’ of path  $p_{cd}$  is simply the smallest pairwise fuzzy affinity along this path. The strength of connectedness  $\mu_K(c, d)$  of the given

pair  $(c, d)$  of voxels in  $C$  is simply the largest of the strength of connectedness of all possible paths in  $\mathcal{C}$  between  $c$  and  $d$ .

*Fuzzy connected object* ( $\mathcal{O}$ ). Such an object  $\mathcal{O}$  in  $\mathcal{C}$  of strength  $\theta_x = [x, 1]$  ( $0 \leq x \leq 1$ ), and containing a voxel  $o$ , consists of a pool  $O \subset C$  of voxels together with a value indicating ‘objectness’ assigned to every voxel.  $O$  is such that  $o \in O$ , and for any voxel  $c \in O$  and  $d \in O$ , the strength of connectedness between them  $\mu_K(c, d) \geq x$ , and for any voxels  $c \in O$  and  $e \notin O$ , the strength  $\mu_K(c, e) < x$ . There are several choices as to how to assign objectness to voxels in  $O$  as described in [21,22,24,25].

Practical algorithms based on dynamic programming have been developed for extracting fuzzy connected objects in two-, three- and higher-dimensional scenes. Our artery–vein separation [19–22] uses such an algorithm called  $\kappa$ FOE and its scale-based version published in Refs. [24, 25]. For a given scene  $\mathcal{C}$ , an affinity  $\kappa$  and a voxel  $o$  in  $C$ , this algorithm outputs a scene called *connectivity scene*  $\mathcal{C}_{K_o} = (C, f_{K_o})$ , wherein for any voxel  $c \in C$ ,  $f_{K_o}(c) = \mu_K(o, c)$ .

## 2.3. Relative fuzzy connectedness

Instead of defining an object on its own based on the strength of connectedness (as in absolute fuzzy connectedness), all other objects (co-objects) of importance that are present in the scene are also considered and all objects are let to compete among themselves in having voxels as their members in relative fuzzy connectedness. In this competition, every pair of voxels in the scene will have a strength of connectedness in each object. The object in which this strength is highest will claim membership of the voxels. This approach of fuzzy object definition using relative strength of connectedness eliminates the need for a threshold of strength of connectedness  $\theta_x$  that is part of the previous definition described above. It is more natural since it relies on the fact that an object gets defined in a scene by the presence of other objects that coexist in the scene. All specified objects are defined simultaneously in this approach.

*Relative fuzzy connectedness* ( $\mu_K(a, c), \mu_K(v, c)$ ). For simplicity, a scene which consists of one object and a background is considered here, although this can be generalized to multiple objects. In our application, the arteries constitute the object and the veins the background. For any voxels  $a$  in the object region (artery) and  $v$  in the background (vein), we define

$$P_{av_\kappa} = \{c | c \in C \text{ and } \mu_K(a, c) > \mu_K(v, c)\}. \quad (3)$$

*Relative fuzzy connected object* ( $\mathcal{O}$ ). Such an object in  $\mathcal{C}$  containing a voxel  $a$  relative to a background containing a voxel  $v$  is a fuzzy subset of  $C$  defined

by the membership function

$$\mu_{\mathcal{O}}(c) = \begin{cases} \eta(f(c)), & c \in P_{av_\kappa}, \\ 0, & \text{otherwise.} \end{cases} \quad (4)$$

where  $\eta$  is an ‘objectness’ function with  $[0,1]$  as its range as described in Refs. [21,22,24,25]. If we are seeking a binary result of segmentation, then  $P_{av_\kappa}$  represents such a result.

*Iterative relative fuzzy connectedness* ( $\mu_\kappa(a, c)$ ,  $\mu_{\kappa_{av}^0}(v, c)$ ). An extension of relative fuzzy connectedness to an iterative framework is described here, which was specifically developed for artery–vein separation. In the following,  $i$  denotes the iteration number. For any fuzzy affinity  $\kappa$  and for any voxels  $c, d \in C$ , we define

$$\mu_{\kappa_{av}^0}(c, d) = \mu_\kappa(c, d), \quad (5)$$

$$P_{av_\kappa}^0 = \{c | c \in C \text{ and } \mu_\kappa(a, c) > \mu_{\kappa_{av}^0}(v, c)\}. \quad (6)$$

For any integer  $i(1, 2, \dots)$ , define

$$\mu_{\kappa_{av}^i}(c, d) = \begin{cases} 1, & \text{if } c = d, \\ 0, & \text{if } c \text{ or } d \in P_{av_\kappa}^{i-1}, \\ \mu_\kappa(c, d), & \text{otherwise.} \end{cases} \quad (7)$$

$$P_{av_\kappa}^i = \{c | c \in C \text{ and } \mu_\kappa(a, c) > \mu_{\kappa_{av}^i}(v, c)\}. \quad (8)$$

$P_{av_\kappa}^0$  is the same as  $P_{av_\kappa}$  and can be delineated using relative fuzzy connectedness first. Once it is identified, it will be excluded from consideration in the subsequent iterations for any path from  $v$  to  $c$  to pass through. In this way we can substantially weaken the strongest path from  $v$  to  $c$  compared to the strongest path from  $a$  to  $c$  which is still allowed to pass through  $P_{av_\kappa}^0$ . This leads us to an iterative strategy to grow from  $a$  (and so complementarily from  $v$ ) to more accurately capture the object (and the background) than if a single-shot relative fuzzy connectedness strategy is used.

*Iterative relative fuzzy connected object* ( $\mathcal{O}_{av_\kappa}^i$ ). Such an object in  $\mathcal{C}$  containing a voxel  $a$  relative to a background containing a voxel  $v$  is a fuzzy subset of  $C$  defined by the membership function

$$\mu_{\mathcal{O}_{av_\kappa}^i}(c) = \begin{cases} \eta(f(c)), & c \in P_{av_\kappa}^i, \\ 0, & \text{otherwise.} \end{cases} \quad (9)$$

An algorithm called  $\kappa$ IRFOE for extracting a relative fuzzy connected object  $\mathcal{O}$  of  $\mathcal{C}$  containing a voxel  $a$  relative to a background containing a voxel  $v$  has been developed [27]. This algorithm works in an iterative fashion and terminates in a finite number of iterations when there is no change in membership between artery and vein.

### 3. Methods

This section describes a complete procedure for implementing artery–vein separation by utilizing the principles

and algorithms shown in Section 2. This procedure consists of the following five major steps: (1) converting data from DICOM3 to 3DVIEWNIX format, (2) previewing slices and creating VOI and MIP Shell, (3) segmenting vessel, (4) separating artery and vein, and (5) shell rendering vascular structures and creating animations. These steps are described in more detail below.

#### 3.1. Converting data from DICOM3 to 3DVIEWNIX format

There are many vendors of imaging devices and there are also many modalities. Vendors follow their own formats of scene data representation. Proprietary restrictions on these formats pose special difficulties for using software packages such as 3DVIEWNIX-AVS. These difficulties, combined with the fact that different computing platforms may have different byte ordering for the different types of data entities, make scene data access really a vexing problem [23]. We adopt the standard DICOM3 (suggested by ACR-NEMA) as the only solution to this problem, and developed a DICOM3–3DVIEWNIX conversion program to allow bringing scene data into this software package. This program converts multiple 2D scenes in DICOM3 format into a single 3D scene in 3DVIEWNIX format, which is actually a generalization of DICOM3 to multi-dimensions and to other non-image structure data.

#### 3.2. Previewing slices and creating VOI and MIP Shell

Previewing slices of CE-MRA scene provides ways to get an insight on the vascular structures which will facilitate determining the VOI, and to find outliers and exclude them from the VOI. For most CE-MRA scenes, vessels occupy only a part of the field of view. Thus, creating a proper VOI will remove unwanted background regions, greatly reduce the size of scene data, and therefore shorten the processing time.

In spite of its many drawbacks—presence of clutter in display due to other overlapping structures and noise, and lack of information about structural juxtaposition and constitution—MIP is the only form of volume rendering that does not require image segmentation. As the beginning step of artery–vein separation, therefore we use MIP rendering of the given CE-MRA scene without any modification to generate a 3D display as a guidance for the subsequent steps.

A MIP rendition is created by assigning to every pixel in the rendition a value which represents the maximum of the intensities of all voxels which project onto p. To speed up rendering, we project only those voxels whose intensities are above a low threshold value. In our software, this low threshold is fixed at a value corresponding to the 97 percentile of CE-MRA (VOI) scene. It is unified to all CE-MRA image data in our artery–vein separation studies. The left in Fig. 1 shows

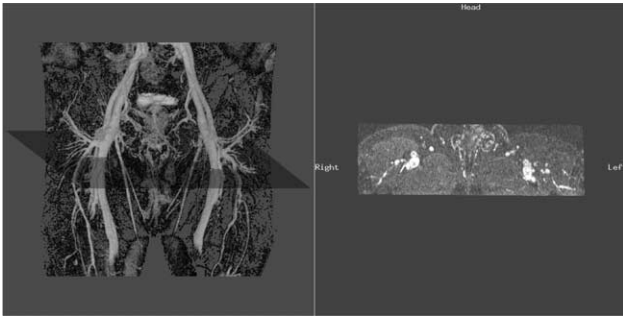


Fig. 1. Specifying seed voxels for segmenting the entire vessel structure and separating artery and vein structures. In the left a Shell rendition of the entire vessel scene is shown. An axial plane is interactively selected. This plane can be positioned precisely by stepping in specified increments. The computed 'slice' at that location is shown on the right. Pairs of seed voxels for artery and vein are specified on these slices.

a MIP rendition. For the description below, we denote the given CE-MRA scene by  $\mathcal{C} = (C, f)$ .

### 3.3. Segmenting vessel

It is tempting to be able to specify the seed voxels directly on the MIP rendition since it is more intuitive. However, such a specification is error prone since the voxel appearing to be in the vessel in the rendition may be a bright noisy voxel in  $\mathcal{C}$ , not in any vessel proper. Therefore, in our implementation, an operator deposits seed voxels on some slices of  $\mathcal{C}$  (the right-hand side of Fig. 1) which correspond to cross-sections at planes selected interactively by operator guided by the MIP rendition of  $\mathcal{C}$  (Fig. 1). Seed voxel specification requires minimal anatomic knowledge of the vascular system as seen in MIP renditions. Thus, when seed voxels are specified, they are stored in two separate sets, one for artery and another for vein.

In this step, algorithm  $\kappa FOE$  of Section 2.2 is applied to  $\mathcal{C}$  to segment the entire vessel structure. The output of the algorithm is a connectivity scene  $\mathcal{C}_{K_0} = (C, f_{K_0})$ . By thresholding this scene at a threshold  $t$ , a new scene  $\mathcal{C}_v = (C, f_v)$  is generated that contains the vessel structure as a fuzzy object, where for any  $c \in C$ ,  $f_v(c) = f_{K_0}(c)$  if  $f_{K_0}(c) \geq t$  and  $f_v(c) = 0$  otherwise. A binary scene  $\mathcal{C}_v^b = (C, f_v^b)$  is also created by thresholding  $\mathcal{C}_{K_0}$  at  $t$  as well as a gray-level scene  $\mathcal{C}_v^g = (C, f_v^g)$ , where for any  $c \in C$ ,  $f_v^g(c) = f(c)$  if  $f_{K_0}(c) \geq t$  and  $f_v^g(c) = 0$  otherwise.

At the very beginning of this development, we randomly selected 10 data sets and tried to determine a fixed threshold  $t$  for all connectivity scenes  $\mathcal{C}_{K_0} = (C, f_{K_0})$ . Quickly, we found that such a fixed threshold  $t$  (optimum for all connectivity scenes) does not exist. Instead, we found that the threshold selected corresponding to the 97 percentile of the connectivity scene works effectively. This value (97 percentile) was determined experimentally based on these 10 data sets and further verified by 133 pelvic and 2 carotid studies. It balances maximizing the completeness

of the vessel structure and minimizing the effects due to artifacts in CE-MRA images.

### 3.4. Separating artery and vein

In the CE-MRA data that we have been dealing with in this project (mostly of the vessels in the region from the pelvis to the knee), most of the vessels run parallel to the MR acquisition plane (coronal). This decision about acquisition planes was made to minimize the acquisition time and still cover a large body region, although from the vessel separation point of view, axial planes would have been more effective. The planes for obtaining the cross-sections (displayed on the right-hand side in Fig. 1) are selected interactively and the end voxels are indicated on the cross-sectional slices. As in the step of *Segmenting vessel*, it would be more intuitive to select voxels directly on the shell renditions of vessels. Unfortunately, the voxels so indicated are in the fuzzy boundary of the vessels and it is difficult to guarantee that these voxels would lie inside the vessels properly. This in turn leads to improper vessel separation. Our initial attempts to steer these points from the fuzzy boundary to the vessel interior proper algorithmically were not successful (although there may be ways of achieving this in the future). Hence we chose the method showed in Fig. 1.

For effective artery–vein separation, we found out in our experiments that many seed voxels are needed in both arteries and veins. This is especially because the major branches are situated very close to each other and often intertwine. The method we found most effective requiring minimum user assistance is to have the operator specify a pair of 'end voxels' specifying segments of major branches of arteries and veins, and then to have an algorithm find a 'central line' running between the end voxels in each pair. Subsequently, all voxels constituting the central line are utilized as seed voxels (Fig. 2). As indicated in the step of *Segmenting vessel*, the user has to specify seed voxels only once instead of two times. When seed voxels are thus specified, they are stored in two separate lists, one for arteries and another for veins. These are then utilized for generating the central lines.

To find the central lines, we first convert the vessel-only binary scene  $\mathcal{C}_v^b$  into a gray scene  $\mathcal{C}_v^d$  by applying a 3D distance transform [28,29] to  $\mathcal{C}_v^b$ . A minimum cost path is then generated between every pair of end voxels utilizing  $\mathcal{C}_v^d$  and an algorithm akin to 'live wire' [30–32] based on dynamic programming. A graph is created for this purpose in which its nodes are the voxels with value 1 (1-voxel) in  $\mathcal{C}_v^b$ , and the arcs indicate that the voxels are 6-adjacent (i.e. they differ in exactly one of their coordinates by 1). A cost is assigned to each arc as follows. For any 1-voxel  $c$  in  $\mathcal{C}_v^b$ , let  $N_+(c)$  denote the number of 1-voxels  $c'$  in the  $3 \times 3 \times 3$  neighborhood of  $c$  such that  $\mathcal{C}_v^d(c') > \mathcal{C}_v^d(c)$ . Analogously, let  $N_-(c)$  denote the number of voxels  $c''$  such that  $\mathcal{C}_v^d(c'') < \mathcal{C}_v^d(c)$ . Then the number  $N(c) = N_-(c) - N_+(c)$

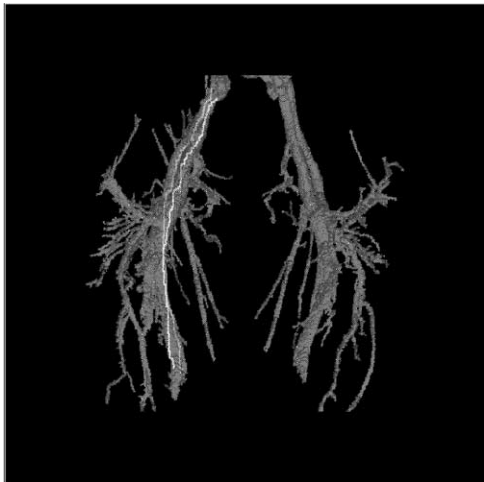


Fig. 2. Two seed voxels have been specified—one inside an artery cross-section at the top end and another within the artery cross-section at the bottom end. The central line generated as a minimum cost path between these two voxels is displayed. All voxels in the central line are utilized as seeds for vessel separation. A central line generated analogously within the vein also is displayed.

is assigned to  $c$ . In this way, a local maximum scene is created. Finally the cost assigned to an arc connecting two voxels  $c$  and  $d$  is  $53 - N(c) - N(d)$ . The best path will go through those voxels (from the starting to the ending) which have the local maximum distance value.

The scene used as input to the iterative relative fuzzy connectedness algorithm is the vessel-only scene  $\mathcal{C}_v^g$ . When artery is chosen as a relative fuzzy connected object, the vein will be considered as the background, or as a relative fuzzy connected co-object. As there is not much intensity difference between voxels inside arteries and those inside veins, object feature based components of affinity is not useful in separating arteries and veins. The same constructions of scale and homogeneity as described in Section 2.1 are used. Instead of Eq. (2), the following equation is used for affinity

$$\mu_\kappa(c, d) = \mu_\alpha(c, d)\mu_{\psi_s}(c, d). \quad (10)$$

Two sets of seed voxels specified inside each of these two objects as described above are utilized for artery–vein separation by applying algorithm  $\kappa IRFOE$ . This algorithm works in an iterative fashion: the small regions of the bigger aspects of artery and vein are separated in the initial iterations, and further detailed aspects of artery and vein are included in later iterations. It terminates in a finite number of iterations when there is no change in membership between artery and vein. In our artery–vein separation studies, the number of iterations is fixed at 7.

Two binary scenes  $\mathcal{C}_A^b$  and  $\mathcal{C}_V^b$  corresponding to  $P_{av_\kappa}^i$  and  $P_{va_\kappa}^i$  and representing relative fuzzy connected artery and vein are output when the iterative process terminates. Using the two binary scenes to mask the vessel-only scene  $\mathcal{C}_v^g$ , artery and vein objects,  $\mathcal{C}_{av_\kappa}^i$  and  $\mathcal{C}_{va_\kappa}^i$  are generated as two

scenes  $\mathcal{C}_A^g = (C, f_A^g)$  and  $\mathcal{C}_V^g = (C, f_V^g)$  defined as follows. For any  $c \in C$ , if  $f_A^b(c) = 1$ ,  $f_A^g(c) = f_V^g(c)$ ; otherwise  $f_A^g(c) = 0$ .  $f_V^g(c)$  is determined analogously.

### 3.5. Shell rendering vascular structures and creating animations

A ‘shell’ is a data structure for representing fuzzy objects and fuzzy boundaries [33]. It typically contains just the voxels that make a non-negligible contribution to the volume rendition of the object. Thus shell has usually a ‘small thickness’ rather than covering the entire scene domain, although in the extreme case, it can be made to cover the entire scene domain. It has been shown to be much faster than volume rendering techniques based on ray casting, but with no noticeable loss in the quality of rendering [33]. We do shell rendering of the entire vessel structure directly from the scene  $\mathcal{C}_v$  obtained in the step of *Segmenting vessel*.

$\mathcal{C}_A^g$  and  $\mathcal{C}_V^g$  in the step of *Separating artery and vein* are used for shell rendering the arteries and veins, respectively. For distinguishing arteries and veins in the display, the shell renditions can be colored differently for the two objects in a composite display or the objects can be turned ‘on’ and ‘off’ selectively. Shell rendering retains object heterogeneity, and therefore, object composition can be more accurately depicted.

## 4. Software package 3DVIEWNIX-AVS

Based on the theory (Section 2) and the methods (Section 3), a software package termed 3DVIEWNIX-AVS has been developed. It integrates 32 computational and operational routines in the five steps described in Section 3 into one single package. Table 1 shows the data flow among these five steps.

In Table 1, files with the extensions *dcm*, *IM0*, *BIM*, and *SH0* represent the files containing the images in DICOM format, scene data, binary scenes, and the structure data of type Shell0, respectively, as defined in the publicly available 3DVIEWNIX software system [23]. Files with the name *scale*, *affinity*, *conn*, and *thrsld* denote the files containing scale data, affinity data, connectivity data, and the scenes by thresholding. *distrs.IM0* and *locmax.IM0* are the files containing the distance transform and local maximum scenes. The locations of seed voxels are stored in the file *path-ends* for vessel segmentation and in the files *artery-path* and *vein-path* for artery–vein separation. The notations in the parenthesis such as  $\mathcal{C}$ ,  $\mathcal{C}_v$ ,  $\mathcal{C}_v^b$ ,  $\mathcal{C}_v^g$ ,  $\mathcal{C}_v^d$ ,  $\mathcal{C}_A$ ,  $\mathcal{C}_A^g$ ,  $\mathcal{C}_V^b$ ,  $\mathcal{C}_V^g$  denote symbols used for the various entities in Sections 2 and 3. The table shows the correspondence between these symbols and the data files.

Since this software package is fashioned after 3DVIEWNIX, its appearance resembles that of 3DVIEWNIX. By selecting items from the menu bar (or from the sub-menu

Table 1  
Data flow in 3DVIEWNIX-AVS

	Operation	Input	Intermediate	Output
1	Data conversion	$mra.dcm_i (i = 1, \dots, n)$		$mra.IMO$
2	VOI creation MIP rendition	$mra.IMO$		$voi.IMO (\mathcal{C})$ $voi.SHO$
3	Vessel segmentation	$voi.IMO$ $voi.SHO$ $path-ends$	$scale.IMO$ $affinity_x.IMO$ $affinity_y.IMO$ $affinity_z.IMO$ $conn.IMO (\mathcal{C}_v)$ $thrsld.BIM \mathcal{C}_v^b$ $distrs.IMO \mathcal{C}_v^d$ $locmax.IMO$	$vessel.IMO \mathcal{C}_v^s$
4	Artery–vein separation	$thrsld.BIM$ $path-ends$ $vessel.IMO$	$artery-path$ $vein-path$ $artery.IMO \mathcal{C}_A^b$ $vein.IMO \mathcal{C}_V^b$	$artery.IMO \mathcal{C}_A^s$ $vein.IMO \mathcal{C}_V^s$
5	Shell rendition	$vessel.IMO$ $artery.IMO$ $vein.IMO$		$vessel.SHO$ $artery-vein.SHO$

bars), user can pick input files and the desired operation, then by clicking on a save button, the results corresponding to that operation will be generated in the output files. The current version of this package can be run in two ways. The first method is a two-step approach: segmenting the entire vessel structure from CE-MRA scene and then separating artery from vein within this vessel structure, i.e.  $voi.IMO \rightarrow vessel.IMO \rightarrow artery.IMO/vein.IMO$ . The second method is a one-step approach: separating artery from vein directly from CE-MRA scene, i.e.  $voi.IMO \rightarrow artery.IMO/vein.IMO$ .

Two manuals, a User Manual and a Reference Manual, are available. The User Manual guides the user step by step in the artery–vein separation process. Radiologic technicians can run this process with a quick training. The Reference Manual shows

- (a) how the package (3DVIEWNIX-AVS) works step by step, and
- (b) what files are used (in) and created (out) at each step.

Following the Reference Manual, users can perform more tasks beyond the default settings of this package. They can directly execute either the partial or the entire (modified) scripts for their specific goals.<sup>3</sup> For instance, users can

- (a) select more start–end voxels and create additional paths as extra seeds (which are particularly helpful for separating higher-order branches of artery and vein),
- (b) perform more iterations and check if the iterations should be terminated for good,

<sup>3</sup> Everytime users use this package and complete a meaningful run, a set of scripts is generated.

- (c) select files and use them under 3DVIEWNIX for further processing by utilizing the functions available in 3DVIEWNIX but not in 3DVIEWNIX-AVS.

### 5. Results

This package has been applied to EPIX Medical, Inc’s CE-MRA data (AngioMark MS-325). One hundred and thirty-five original CE-MRA data sets (of 52 patients) from 6 university hospitals have been processed so far. Among them, 133 scene data pertain to the vessels in the region from the belly to the knee (pelvis) and the other 2 scene data to the vessels in the region of the neck (carotid). CE-MRA data were acquired during the pre-contrast, dynamic (arterial phase), early and late post-contrast (steady-state phases), with various resolutions and orientations, stored in DICOM format. In all our studies, however, only the steady-state data were used since we found in our preliminary experiments that they produce the best segmentations. In all studies, in spite of the variations in the acquisition protocol, we were able to use unified parameter settings for segmentation and rendering without requiring per-study adjustments. All studies were performed on a Gateway 2000 300 MHz/256 MB memory Pentium PC running under Linux. The whole procedure, which includes vessel segmentation, artery–vein separation, and shell rendering,

Table 2  
CE-MRA image data information

Example	Location	Size	Resolution (mm)
1	Pelvis	$512 \times 512 \times 128$	$0.88 \times 0.88 \times 0.75$
2	Carotid	$512 \times 512 \times 123$	$0.47 \times 0.47 \times 0.80$

are completed in 3 min per study including computational and operator time.

Two examples—a pelvis and a carotid image—are presented here to demonstrate the performance of this

approach. For these examples, CE-MRA image data information is given in Table 2. The original CE-MRA scene (one slice), its MIP rendition, a rendition of the segmented vessel, the composite artery–vein

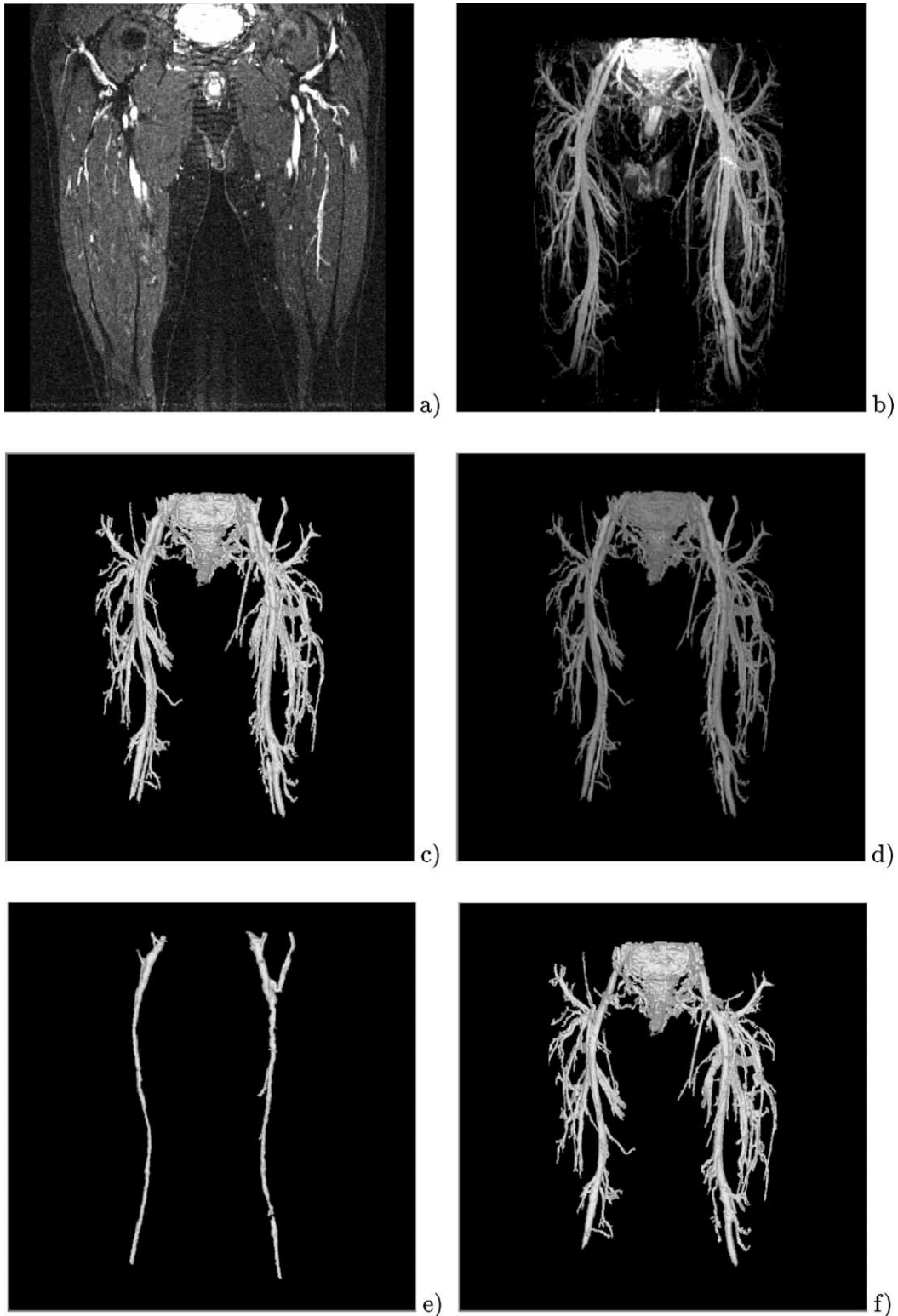


Fig. 3. Example 1: (a) CE-MRA, (b) MIP and shell renditions of (c) vessel, (d) artery–vein, (e) artery, (f) vein.

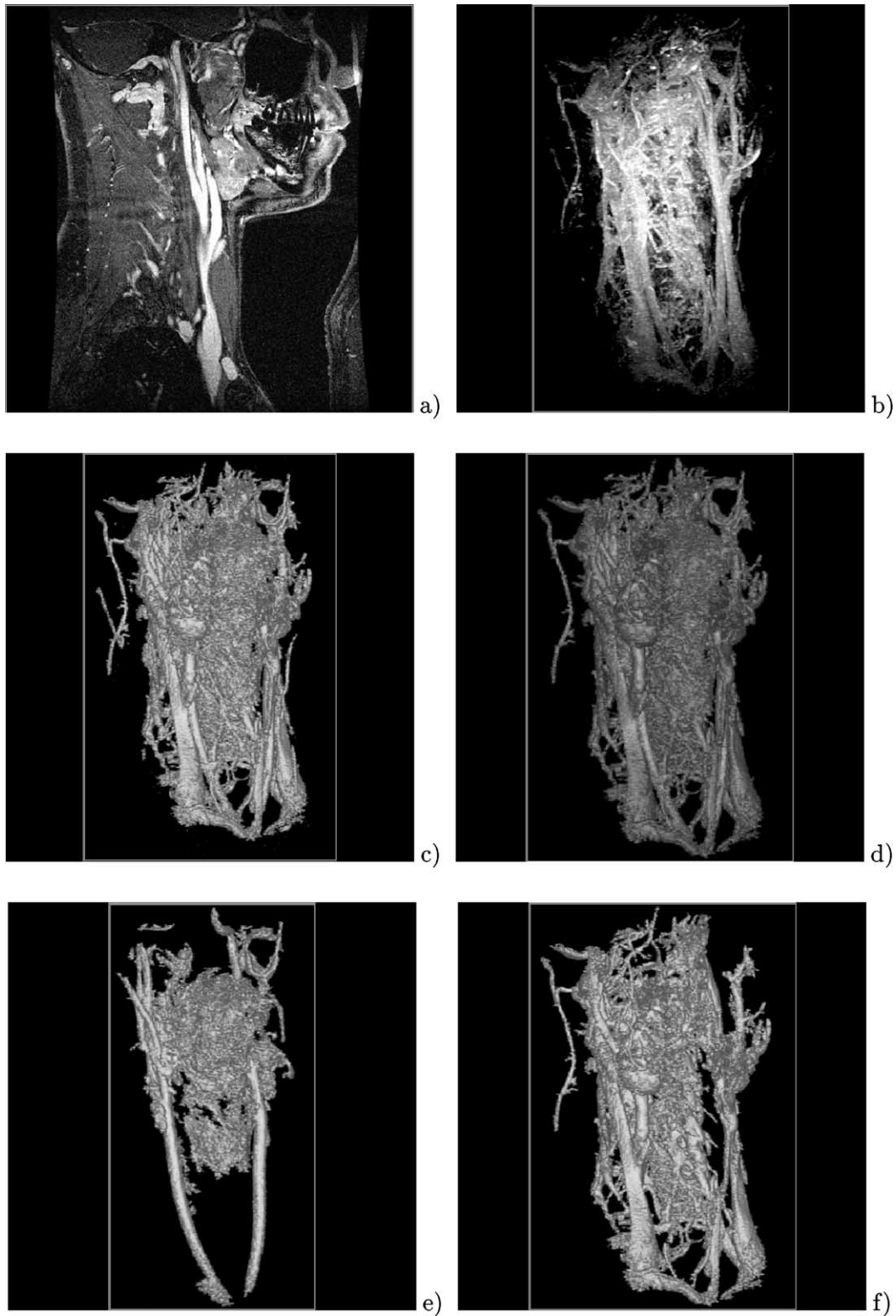


Fig. 4. Example 2: (a) CE-MRA, (b) MIP and shell renditions of (c) vessel, (d) artery-vein, (e) artery, (f) vein.

rendition, and the separated artery/vein renditions are shown in Figs. 3a–4a, 3b–4b, 3c–4c, 3d–4d, 3e–4e, and 3f–4f, respectively. By visual examination of the displays in Figs. 3b–3c and 4b–4c, we find that the majority of vessels

are correctly segmented by this package. Only a few tiny vessels are not included. By examining the displays in Figs. 3e–3f and 4e–4f, we observe that artery-vein separation appears to be qualitatively mostly correct.

## 6. Conclusion

CE-MRA has fundamentally changed angiography and established itself as an important technique complementary to conventional angiography. However, this technique requires advanced vascular visualization as a necessary part of its clinical protocols. Its utility can be significantly enhanced for evaluation and treatment of diseases when artery and vein structures are separated. Our package, by combining the strengths of fuzzy connected object definition, object separation, and shell rendering, provides a high-quality 3D display of vascular information in a single CE-MRA data set that can be used routinely for clinical vascular imaging.

The strengths of this software package are (1) minimal user interaction, (2) minimal anatomic knowledge requirements on human vascular system, (3) clinically required speed, (4) free entry to any operational stages, (5) reproducible, reliable, high quality of results, and (6) cost effective computer implementation. To date, it seems to be the only software package (using an image processing approach) available for artery and vein separation for the routine use in a clinical setting [13–18,34,35].

Several further improvements of this software package have been planned based on our initial experience and are currently being incorporated. To improve the efficiency of this package, we propose (1) a method akin to the Live Wire process [30–32] to simplify seed point selection and path creation, and (2) using a buffer to replace the auxiliary/intermediate files output. Thus, both operation and computation time can be further reduced. For improving visualization of vascular structures and/or anomalies, rendering based on two scale-based filtering methods [36] (scale-based averaging and scale-based diffusion) that use local structure size information to arrest smoothing around fine structures and across even low-gradient boundaries is also planned.

## 7. Summary

CE-MRA has fundamentally changed angiography and established itself as an important technique complementary to conventional angiography. However, this technique requires advanced vascular visualization as a necessary part of its clinical protocols. Its utility can be significantly enhanced for evaluation and treatment of diseases when artery and vein structures are separated.

Our earlier study developed a computerized method, based on fuzzy connected object delineation principles and algorithms, for artery and vein separation in CE-MRA images. This paper reports its current development—a software package—for routine clinical use. The software package, termed 3DVIEWNIX-AVS, consists of the following major operational parts: (1) converting data from DICOM3 to 3DVIEWNIX format, (2) previewing

slices and creating VOI and MIP Shell, (3) segmenting vessel, (4) separating artery and vein, (5) shell rendering vascular structures and creating animations.

This package has been applied to EPIX Medical Inc's CE-MRA data (AngioMark MS-325). One hundred and thirty-five original CE-MRA data sets (of 52 patients) from 6 hospitals have been processed. In all case studies, unified parameter settings produce correct artery–vein separation. The current package is running on a Pentium PC under Linux and the total computation time per study is about 3 min.

The strengths of this software package are (1) minimal user interaction, (2) minimal anatomic knowledge requirements on human vascular system, (3) clinically required speed, (4) free entry to any operational stages, (5) reproducible, reliable, high quality of results, and (6) cost effective computer implementation. To date, it seems to be the only software package (using an image processing approach) available for artery and vein separation of the human vascular system for routine use in a clinical setting.

Several further improvements of this software package have been planned based on our initial experience and are currently being incorporated. To improve the efficiency of this package, we propose (1) a method akin to the Live Wire process [30–32] to simplify seed point selection and path creation, and (2) using a buffer to replace the auxiliary/intermediate files output. Thus, both operation and computation time can be further reduced. For improving visualization of vascular structures and/or anomalies, rendering based on two scale-based filtering methods [36] (scale-based averaging and scale-based diffusion) that use local structure size information to arrest smoothing around fine structures and across even low-gradient boundaries is also planned.

## Acknowledgements

This work has been supported by a contract from EPIX Medical, Inc. The work of JKU, DO, and PKS is supported by NIH grants NS 37172 and AR 46902. The authors are grateful to Drs. Satish Tadikonda and E. Kent Yucel for the CE-MRA data sets and help with manual segmentation and Mr. Mike Hartmann and Mr. Robert Stefancik for help with the project at various stages.

## References

- [1] Priatna A, Paschal CB. Variable-angle uniform signal excitation (VUSE) for three-dimensional time-of-flight MR angiography. *JMRI* 1995;5(4):421–7.
- [2] Kutka R, Stier S. Extraction of line properties based on direction field. *IEEE Trans Med Imaging* 1996;15(1):51–8.

- [3] Balaban RS, Chesnick S, Hedges K, Samaha F, Heineman FW. Magnetization transfer contrast in MR imaging of heart. *Radiology* 1991;180(3):671–5.
- [4] Ekelund I, Sjoqvist K-A, Asberg B. MR angiography of abdominal and peripheral arteries. *Acta Radiol* 1996;37:3–13.
- [5] Prince M. Gadolinium-enhanced MR angiography. *Radiology* 1994;191(1):155–64.
- [6] Thurnher SA, Dorffner R, Thurnher MM, Kretschmer G, Pilzauer P, Lammer J. Evaluation of abdominal aortic aneurysm for stent-grafting: contrast-enhanced 3D-tof angiography versus 3D CT angiography versus digital subtraction angiography. *Radiology* 1997;205(Suppl):1564.
- [7] Lebowitz JA, Rofsky NM, Krinsky GA, Weinreb JC. Gadolinium-enhanced body MR venography with subtraction technique. *Am J Roentgenol* 1997;169(3):755–8.
- [8] Lauffer RB, Parmelee DJ, Dunham SU, Ouellet HS, Dolan RP, Witte S, McMurry TJ, Walovitch RC. MS-325: albumin-targeted contrast agent for MR angiography. *Radiology* 1998;207(2):529–38.
- [9] Grist TM, Korosec FR, Peters DC, Witte S, Walovitch RC, Dolan RP, Bridson WE, Yucel EK, Mistretta CA. Steady-state and dynamic MR angiography with MS-325: initial experience in humans. *Radiology* 1998;207(2):539–44.
- [10] Engelbrecht MR, Saeed M, Wendland MF, Canet E, Oksendal AN, Higgins CB. Contrast-enhanced 3D-TOF MRA of peripheral vessels: intravascular versus extracellular MR contrast media. *J Magn Reson Imaging* 1998;8(3):616–21.
- [11] Stillman AE, Wilke N, Li D, Haacke M, McLachlan S. Ultrasmall superparamagnetic iron oxide to enhance MRA of the renal and coronary arteries: studies in human patients. *J Comput Assist Tomography* 1996;20:51–5.
- [12] Yucel EK. Visualization techniques for blood-pool contrast agent enhanced magnetic resonance angiography. *CMR '99 Proceedings*; 1999.
- [13] Bluenke DA, Darrow RD, Gupta R, Tadikonda SK, Dormoulin CL. 3D contrast enhanced phase contrast angiography: utility for arterial/venous segmentation. *ISMRM Proc* 1999;2:1237.
- [14] Mazaheri Y, Carroll TJ, Mistretta CA, Korosec FR, Grist TM. Vessel segmentation in 3D MR angiography using time resolved acquisition curves. *ISMRM Proc* 1999;3:2181.
- [15] Foo TKF, Ho V, Hood MN, Czum JM, Wolf SD, Zhang Y, Choyke PL. A novel method for MR arterial and venous discrimination using gated phase contrast and VENC selection. *ISMRM Proc* 1999;3:2182.
- [16] Bock M, Schoenberg SO, Flomer F, Grau A, Strecker R, Schad LR. Artery–vein separation in 3D contrast enhanced pulmonary MRA using correlation. *ISMRM Proc* 1999;1:486.
- [17] Sonka M, Stefancik R, Tadikonda S. Feasibility of automated separation of arteries and veins using a graph searching. *ISMRM Proc* 1999;3:2183.
- [18] Niessen W, van Swijndregt AM, Elsmann B, Wink O, Viergever M, Mali W. Enhanced artery visualization in blood pool MRA: results in the peripheral vasculature. *IPMI Proc* 1999;1613:340–5.
- [19] Lei T, Udupa JK, Saha PK, Odhner D. 3D MR angiographic visualization and artery–vein separation. *SPIE Proc* 1999;3658:52–9.
- [20] Lei T, Udupa JK, Saha PK, Odhner D. Separation of artery and vein in contrast enhanced MRA images. *SPIE Proc* 2000;3978:233–44.
- [21] Lei T, Udupa JK, Odhner D, Saha PK. 3dviewnix-avs: a software package for separate visualization of arteries and veins in CE-MRA images. *SPIE Proc* 2001;4319:515–24.
- [22] Lei T, Udupa JK, Saha PK, Odhner D. Artery–vein separation via MRA: an image processing approach. *IEEE Trans Med Imaging* 2001;20(8):689–703.
- [23] Udupa JK, Odhner D, Samarasekera S, Goncalves G, Iyer K, Venugopal K, Furuie S. 3DVIEWS: an open, transportable, multidimensional, multimodality, multiparametric imaging software system. *SPIE Proc* 1994;2164:58–73.
- [24] Udupa JK, Samarasekera S. Fuzzy connectedness and object delineation: theory, algorithm, and applications in image segmentation. *Graph Models Image Process* 1996;58(3):246–61.
- [25] Saha PK, Udupa JK, Odhner D. Scale-based fuzzy connected image segmentation: theory, algorithm, and validation. *Comput Vision Image Understand* 2000;77:145–74.
- [26] Saha PK, Udupa JK, Lutofu A. Relative fuzzy connectedness and object definition: theory, algorithms, and applications in image segmentation. Technical Report, vol. MIPG 265; 1999.
- [27] Saha PK, Udupa JK. Iterative relative fuzzy connectedness and object definition: theory, algorithms, and applications in image segmentation. *Proceedings of IEEE Workshop on Mathematical Methods in Biomedical Image Analysis*; 2000. p. 28–35.
- [28] Borgefors G. On digital distance transform in three dimensions. *Comput Vision Image Understand* 1996;64(3):368–76.
- [29] Zhang S, Karim MA. Euclidean distance transform by stack filters. *IEEE Signal Process Lett* 1999;6(10):253–6.
- [30] Falcao AX, Udupa JK, Samarasekera S, Sharma S, Hirsch BE, Lutofu RA. User-steered image segmentation paradigms: live wire and live lane. *Graph Models Image Process* 1998;60(4):233–60.
- [31] Falcao AX, Udupa JK. A 3D generalization of user-steered live-wire segmentation. *Med Imaging Anal* 2000;4:389–402.
- [32] Falcao AX, Udupa JK, Miyazawa FK. An ultra-fast user-steered image segmentation paradigm: live wire on the fly. *IEEE Trans Med Imaging* 2000;19(1):55–61.
- [33] Udupa JK, Odhner D. Shell rendering. *IEEE Comput Graph Appl* 1993;13(6):58–67.
- [34] Davis C, Ladd M, Romanowski B, Wildermuth S, Knoploch J, Debatin J. Human aorta: preliminary results with virtual endoscopy based on three-dimensional MR imaging data sets. *Radiology* 1996;199:37–40.
- [35] ACR Task Force on Appropriateness Criteria, American college of radiology appropriateness criteria. Reston, VA: American College of Radiology; 1995.
- [36] Saha PK, Udupa JK. Scale-based diffusive filtering of medical images. *SPIE Proc* 2000;3979:735–46.

Tianhy Lei biography not available at time of publication.

**Jayaram K. Udupa** received a PhD in Computer Science in 1976 from the Indian Institute of Science, Bangalore, with a medal for best research. During the past 26 years, he has worked in the areas of biomedical image and signal processing, pattern recognition, biomedical computer graphics, 3D imaging, visualization and their biomedical applications. He has published over 110 journal papers in these areas, over 120 full conference papers, edited two books on 3D imaging, written over 20 book chapters and editorials, given over 120 invited talks (since 1986), offered consultancy to several industries, organized conferences, seminars and workshops, and co-developed the first software package for medical three-dimensional imaging and developed and widely distributed large software systems for 3D imaging. He is a Fellow of the American Institute of Medical and Biological Engineering. He is at present the Chief of the Medical Imaging Section and Professor of Radiological Sciences in the Department of Radiology at the University of Pennsylvania, Philadelphia.

**Dewey Odhner** has been a programmer with the Medical Image Processing Group at the University of Pennsylvania since 1987. He works on design and implementation of new features and maintenance of the 3DVIEWNIX software system for visualization and analysis of 3D biomedical data, and related programs, contributing also to many of the new methods and improved techniques in these programs, including rendering, segmentation, various measurements, and many other tasks. He has also worked on optimization problems and evaluation of image reconstruction algorithms. He earned his MA in physics from Temple University, his BS from Penn State, and his AA from Bryn Athyn College of the New Church. He is a member of Phi Beta Kappa.

**László G. Nyúl** received his BS and MS degree in Computer Science and Mathematics, both with honors, from József Attila University, Szeged, in 1992 and 1994, respectively. Since 1993 he has been with the Department of Applied Informatics, University of Szeged as an assistant lecturer. He teaches university courses in computer graphics, image processing, multimedia. He worked as a research fellow at the Medical Image Processing Group, University of Pennsylvania, between 1998 and 2000. He is author of several journal articles and conference articles. His research interests include medical image processing, segmentation analysis and applications. He is in the final phase of obtaining his PhD degree in Computer Science from the University of Szeged.

**Punam K. Saha** obtained his Bachelor's and Master's degrees in Computer Science and Engineering from Jadavpur University, India, in 1987 and 1989, respectively. In 1997 he received his PhD from the Indian Statistical Institute, which he joined as a faculty member in 1993. In 1997 he joined the University of Pennsylvania, Department of Radiology, Medical Imaging Section, as a Post-doctoral Fellow where he is currently an Assistant Professor. His present research interests include biomedical imaging problems and the application of their solutions, local scale-based image analysis, digital topology and its application to image processing, and estimation of trabecular bone strength from MR images. He has published more than 35 papers in international journals. He received a Young Scientist award from the Indian Science Congress Association in 1996. He is an associate of Pattern Recognition journal and is member of the IEEE and the International Association for Pattern Recognition and a member of the Governing body of the Indian Unit for Pattern Recognition and Artificial Intelligence.